

See discussions, stats, and author profiles for this publication at: <https://www.researchgate.net/publication/231390813>

Measurement of Dynamic Liquid Distributions in a Fixed Bed Using Electrical Capacitance Tomography and Capacitance Wire-Mesh Sensor

ARTICLE *in* INDUSTRIAL & ENGINEERING CHEMISTRY RESEARCH · JANUARY 2010

Impact Factor: 2.59 · DOI: 10.1021/ie900988f

CITATIONS

20

READS

86

4 AUTHORS, INCLUDING:



[Marco Jose Da Silva](#)

Federal Technological University of Paraná...

95 PUBLICATIONS 460 CITATIONS

[SEE PROFILE](#)

Measurement of Dynamic Liquid Distributions in a Fixed Bed Using Electrical Capacitance Tomography and Capacitance Wire-Mesh Sensor

Bartosz Matusiak,^{*,†} Marco Jose da Silva,[†] Uwe Hampel,[†] and Andrzej Romanowski[‡]

Institute of Safety Research, Forschungszentrum Dresden-Rossendorf, Bautzner Landstrasse 400, 01328 Dresden, Germany, and Computer Engineering Department, Technical University of Lodz, Stefanowskiego 18/22, 90924 Lodz, Poland

An intricate problem associated with fixed bed operation is liquid maldistribution, which denotes the fact that the liquid does not homogeneously flow through the bed. In a comparative study we evaluated two capacitance imaging methods—capacitance wire-mesh sensor and electrical capacitance tomography (ECT)—with respect to their capability of measuring static and dynamic liquid holdup in a fixed bed. The capacitance wire-mesh sensor as an invasive instrument is able to disclose flow structures at higher spatial resolution and was therefore considered the reference instrument for liquid holdup measurement. We found that both methods predict dynamic liquid holdup in the column in a similar way with only small systematic deviation. The results therefore prove that noninvasive electrical capacitance tomography can reliably measure cross-sectional dynamic liquid holdup in a fixed bed, even with a simple and fast linear back projection reconstruction algorithm.

1. Introduction

Trickle bed reactors are multiphase reaction devices, where fluids are brought into reaction in a randomly packed bed of catalyst particles. Such reactors are operated, for instance, in the manufacturing of petroleum-based products and in the production of chemicals and pharmaceuticals.^{1,2} The common operation mode in trickle bed reactors is a concurrent downward flow of liquid and gas through the bed, while upward flow operation remains an exception.³ Several flow regimes can exist in a trickle bed reactor, and the flow regime decisively determines the efficiency of heat and mass transfer.⁴ An intricate problem associated with fixed bed operation is liquid maldistribution, which denotes the fact that the liquid does not homogeneously flow through the bed. Liquid maldistribution is an economic issue since some amount of the expensive catalyst does not contribute to the reaction. Moreover, liquid maldistribution may impact the safety of reactor operation for some exothermic reactions. To achieve improved utilization of the catalyst bed and better reactor performances, as well as to meet with rising environmental and safety constraints, hydrodynamics in trickle bed reactors and their coupling to chemical reaction still need examination. Hydrodynamic target parameters of such examinations are axial and cross-sectional liquid distribution, saturation, and pressure drop.^{5,6}

In the past, considerable effort was spent to visualize and characterize multiphase flows in fixed bed reactors. Such investigations are very difficult to conduct due to the opaque nature of fixed beds. For many years investigators have utilized local probes, such as annular liquid collectors installed at the bottom of the bed, differential pressure transducers, tracer methods, thermal or phase indicator probes, and colorimetric techniques.^{7–11} While optical techniques are hardly applicable, tomographic imaging modalities seem to be rather attractive. Thus, Gladden et al.,^{12,13} Koptyug et al.,¹⁴ and Nguyen et al.¹⁵ applied magnetic resonance imaging (MRI), which can disclose the phase fraction distribution with good spatial and temporal resolution. However, MRI is limited to small vessels made of

nonmagnetic materials. X-ray transmission tomography, which was used by Marchot et al.¹⁶ and Van der Merwe et al.,¹⁷ as well as γ -ray transmission tomography, utilized by Boyer et al.¹⁸ and Schubert et al.,¹⁹ are another choices, but suffer from low temporal resolution. Moreover, they are cost-intensive and require radiation shielding and complex mechanics. In terms of complexity and temporal resolution, electrical tomography techniques are to be favored. Depending on the electrical property that is to be imaged, there is a choice between electrical resistance tomography (ERT)²⁰ and electrical capacitance tomography (ECT).²¹ For imaging of gas–liquid flow in a fixed bed, ECT, which reconstructs electrical permittivity, is better suited. The permittivity of a material is given by $\epsilon = \epsilon_0 \epsilon_r$, where $\epsilon_0 \approx 8.85 \times 10^{-12} \text{ A s V}^{-1} \text{ m}^{-1}$ denotes the vacuum permittivity and ϵ_r is the relative permittivity ranging from 1 for gas and vacuum to roughly 80 for water. Organic liquids have intermediate values, for instance $\epsilon_r = 2$ for oil and $\epsilon_r = 20$ for 2-propanol. Measuring permittivity instead of electrical conductivity has some advantages. First, numerous organic liquids, such as oil, are not electrically conducting and cannot be discriminated, e.g., from gas. Second, electrical conductivity of the same liquid, e.g., water, largely depends on the ion concentration, which may vary over many decades, making it difficult to calibrate the sensor.

In general, an ECT system comprises a sensor of 8–32 electrodes which are uniformly arranged on the boundary of a vessel. An associated electronic circuit consecutively measures electrical capacitance between all pairs of electrodes at high speed. The capacitance between two electrodes of indices i and j in turn is related to the relative permittivity distribution $\epsilon(x,y)$ in the cross section by

$$C_{ij} = -\frac{1}{\varphi_j - \varphi_i} \oint_{\Gamma} \epsilon_0 \epsilon_r(x,y) \nabla \varphi(x,y) d\Gamma \quad (1)$$

where φ is the electrical potential and Γ is the area of integration on the detecting electrode. Having obtained a full set of capacitance readings from the ECT sensor, a cross-sectional permittivity image can be computed by applying a so-called image reconstruction algorithm, which numerically seeks a solution $\epsilon_r(x,y)$ by solving the inverse problem associated with eq 1. There is a choice of solution strategies to this inverse

* To whom correspondence should be addressed. E-mail: bmatus@kis.p.lodz.pl

[†] Forschungszentrum Dresden-Rossendorf.

[‡] Technical University of Lodz.

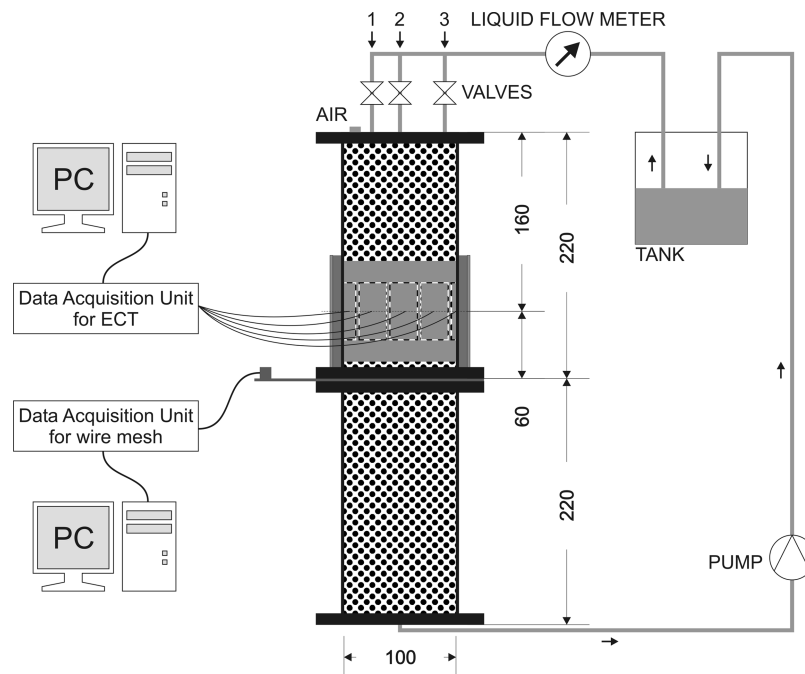


Figure 1. Experimental setup with fixed bed column, media supply, ECT, and wire-mesh sensors.

problem,²² whereby the most popular algorithm is fast linear back projection (LBP). LBP algorithms give a straightforward approximate solution with some compromise in spatial resolution. On the other hand, more sophisticated nonlinear iterative image reconstruction algorithms may be applied, which require higher computational effort but give better results in terms of spatial resolution. In general however, spatial resolution is limited by the soft-field effect, that is, the spread of the electrical field inside the object to maybe 10% of the object diameter. This is a drawback compared to hard-field modalities, such as X-ray or γ -ray computed tomography.

The usability of ECT for the investigation of trickle bed reactors was already considered in the past. Some attempts were made by Reinecke and Mewes.^{23–25} They employed the iterative algebraic reconstruction technique (ART) for image reconstruction, which requires offline data processing and does not allow online observations. Tibirna et al.²⁶ compared reconstruction algorithms for ECT applied to trickle bed reactors, but the tests were performed only for software phantoms. Hamidipour et al.²⁷ recently used ECT to monitor the deposition of fine particles in trickle bed reactors. Furthermore, Warsito and Fan²⁸ proposed a three-phase capacitance model to attain the gas holdup and the solids fraction from the permittivity distribution. However, there is no work so far where ECT measurements have been evaluated or even compared to another imaging modality. Due to the known inherent problems of ECT (low spatial resolution, dependence of quantitative image information on the utilized capacitance model and reconstruction algorithm), this is a missing issue which, we felt, deserves proper attention. In this paper we compared ECT measurements with data from a capacitance wire-mesh sensor, where the latter as an intrusive instrument provided cross-sectional liquid distribution images at superior speed and high spatial resolution. Nonintrusive techniques may be the first choice in the investigation of fixed bed reactors due to the fact that they do not affect the flow in the column. However, all currently available nonintrusive techniques suffer from some limitation such as low spatial or temporal resolution. Thus, the use of intrusive techniques is still the only suitable choice.

The wire-mesh sensor is a powerful intrusive imaging instrument which was introduced by Prasser et al.²⁹ It consists of two planes of wire electrodes stretched across the cross section of a pipe at an angle of 90° for wires of different planes. An associated electronics measures the local conductivity in the gaps of the wire crossings. In contrast to electrical tomography, image reconstruction is no longer needed since the sensing volume is confined to the vicinity of each crossing point. As a consequence, a spatial resolution up to 0.5 mm and online visualization are feasible.³⁰ The applicability of the conductivity wire-mesh sensor for fixed beds was recently demonstrated by Llamas et al.^{31,32} However, with acquisition times in the range of 10–15 s per cross-sectional scan, their system is rather slow and not suited for dynamic holdup measurements. Recently, Da Silva et al.³³ introduced a new type of wire-mesh sensor, based on capacitance instead of conductivity measurements. The capacitance wire-mesh sensor is much better suited for fixed bed studies and was therefore employed in this study.

2. Experimental Setup and Data Processing

2.1. Fixed Bed Test Facility Setup. All experiments were performed on a fixed bed test facility which is schematically shown in Figure 1. A PVC column of 100 mm internal diameter and a height of 440 mm was randomly packed with commercial porous α -Al₂O₃ catalyst spheres (Duranit D99). Relative permittivity for the pure Al₂O₃ is 9.33.³⁴ For the porous particles the bulk relative permittivity value is accordingly lower and was measured between 2.1 and 2.6. Table 1 shows essential

Table 1. Specification of the Bed Particles

catalyst support	α -Al ₂ O ₃
packing shape	spherical pellets (sphericity < 1.25)
average diameter	3.2–4.0 mm
total surface area (BET)	<100 m ² ·kg ⁻¹
internal porosity	≈0.16
packing porosity	≈0.45
bulk density	≈2100 kg·m ⁻³
relative electrical permittivity of pure Al ₂ O ₃	9.33
estimated relative electrical permittivity of used porous particle	2.1–2.6

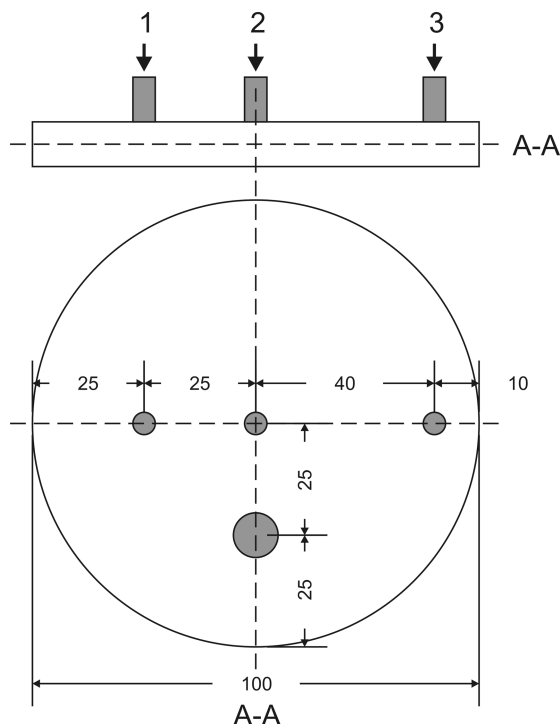


Figure 2. Geometry of the top plate with the three liquid inlets.

properties of the bed particles. The test facility was operated at ambient pressure and room temperature. As a liquid we used 2-propanol (C_3H_8O) with a relative permittivity of 20.18.³⁴ It was admitted through a combination of three individually controllable inlets and then pumped from the bottom outlet to a tank. Geometric details of the top plate with the inlets are shown in Figure 2. Applied volumetric liquid flow rates were 40 and $60 \text{ L} \cdot \text{h}^{-1}$.

According to Gianetto and Specchia³⁵ the liquid distribution at the top of the bed may be different from that in the rest of the bed. Therefore, the ECT sensor was placed 115 mm from the top of the column. Respectively, the wire-mesh sensor was inserted 15 mm underneath the bottom of the ECT sensor. In order to avoid cross-interference, the sensors were sufficiently spaced apart from each other.

2.2. Electrical Capacitance Tomography Setup. The ECT experimental setup consists of the sensor and an ET3 data acquisition unit, which was developed at the Technical University of Warsaw by Olszewski et al.³⁶ This device is operated from a personal computer. The electronics implements a charge-discharge principle for capacitance measurements, in contrast to ac-based measuring schemes implemented in other ECT systems.³⁷ In most applications, the electrodes of the ECT sensors are placed on the outside of the investigated vessel. However, it was shown by Jaworski and Bolton³⁸ that if the

ratio of the permittivity values of the media inside the sensor and the material of the vessel wall is more than about 8, the capacitance measurement records between adjacent electrodes become nonlinearly related to the internal permittivity which hampers correct image reconstruction. This holds for the given case where 2-propanol ($\epsilon_r = 20.18$) has a much higher permittivity than the poly(vinyl chloride) wall ($\epsilon_r = 3.39$) of the column. Hence, we reverted to a special ECT sensor design with isolated internal electrodes. This sensor was made as the flexible printed circuit board (flex-PCB) as shown in Figure 3. The sensor consists of 12 electrodes. Each electrode is 50 mm long and 23.5 mm wide. Above, below, and between electrodes a grounded shield was placed. The flex-PCB is tightly glued inside the column in such a way that electrodes are in contact with the internal surface of the wall. Wire connections to the electrodes were made through holes in the column wall which were sealed with glue after soldering. To prevent electrical influence from the exterior of the column, an additional external grounded shield was provided.

Data acquisition with the ET3 system is about 60 frames per second (fps). Each data set contains 66 independent capacitance values. For the purpose of numerical image reconstruction, a mesh consisting of 1536 triangle elements was prepared with the use of the NETGEN mesh generator (Open Source under LGPL). Since the major objective was the investigation of the ability to use ECT for online flow monitoring and analysis, the basic LBP imaging method was employed to solve the inverse problem. This method is fast and simple. It is based on the approximation that the relationship between measurements and permittivity distribution is linear, which is formally described as

$$\mathbf{C} = \mathbf{S} \cdot \mathbf{G} \quad (2)$$

Here, \mathbf{C} is a vector containing the capacitance measurements, \mathbf{S} is a matrix encoding the sensitivity maps for each electrode pair, and \mathbf{G} is the pixellated permittivity image that is to be reconstructed. There are different methods to obtain the sensitivity maps. In this study, the sensitivity maps were calculated by numerically solving Poisson's equation for the electrical fields.³⁹

An approximate solution using the LBP algorithm is given by

$$\hat{\mathbf{G}} = \mathbf{H} \cdot \mathbf{S}^{-1} \cdot \mathbf{C} \quad (3)$$

where the multiplication by the pseudoinverse of the nonsquare type matrix \mathbf{S} denotes the back projection, \mathbf{H} is a filter applied to correct the back projected image properly, and $\hat{\mathbf{G}}$ denotes the approximate solution.

2.3. Wire-Mesh Sensor Setup. The wire-mesh sensor is composed of two planes with 16 stainless steel wires of 0.1 mm diameter and 6.25 mm separation from each other. The distance between planes is 1.5 mm and the wires from different

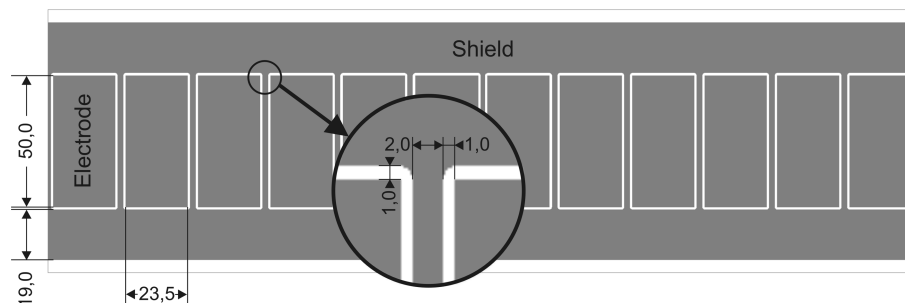


Figure 3. Flexible printed circuit board (flex-PCB) of the experimental ECT sensor.

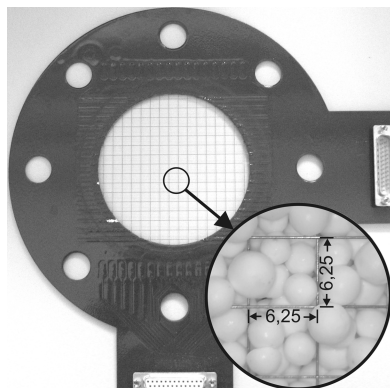


Figure 4. Experimental wire-mesh sensor.

planes run at a right angle. This arrangement gives 208 sensing points inside the circular cross section of the column. The wire-mesh sensor was inserted into the column via a flange and fixed with screws. Since the wires run through the bed, care was given not to disturb the typical bed structure. Therefore, we first filled the lower part of the column with catalyst particles, inserted the sensor afterward, and then carefully filled particles on top of the wire mesh. Figure 4 gives a detailed view of the wire structure inside the bed.

In contrast to the ECT system, the wire-mesh sensor utilizes an ac-based scheme for capacitance measurements with logarithmic detection and demodulation of the ac signal (for details see Da Silva et al.³³). Therefore, the transmitter wires are subsequently excited by ac voltage while the crossing receiver wires receive an ac displacement current. This current signal is amplified and converted into a voltage signal, whose strength is related to the capacitance C in a crossing point by

$$V = a \ln(C) + b \quad (4)$$

Here, a and b are circuit constants which can be determined experimentally. The capacitance itself is linearly related to the permittivity of the material in the wire crossing according to

$$C = \varepsilon_0 \varepsilon_r k_g \quad (5)$$

where k_g is a scaling length factor determined by the wire geometry. Equations 4 and 5 hold for every crossing point. Thus, scanning all crossing points is possible to obtain a matrix \mathbf{G} (in analogy to ECT) representing the capacitance (or permittivity) distribution over the cross section.

The wire-mesh sensor can generate up to 625 fps. In this study it was operated at 100 fps. An image consists of 16×16 pixels, one for each wire crossing point. For improved image quality, cubic interpolation of the measurements to a 32×32 grid was performed.

2.4. Calibration and Data Processing. Both ECT and wire-mesh sensor imaging techniques require proper calibration in order to obtain liquid holdup distributions from measurements. Therefore, reference scans were performed prior to the measurements. First, the dry bed was scanned and acquired capacitance readings were saved as a matrix $\mathbf{C}^{(\text{empty})}$. Note that capacitance readings from the ECT system are integral measurements between electrode pairs according to eq 1 and capacitance readings from the wire-mesh sensor are local measurements according to eqs 4 and 5. Then the bed was completely flooded and scanned after 15 min, yielding a reference $\mathbf{C}^{(\text{flooded})}$. Finally, the bed was drained and the different flows were scanned. This procedure of preparing the experimental trickle bed reactor is also known as Levec prewetting.¹⁷ To compute a liquid holdup

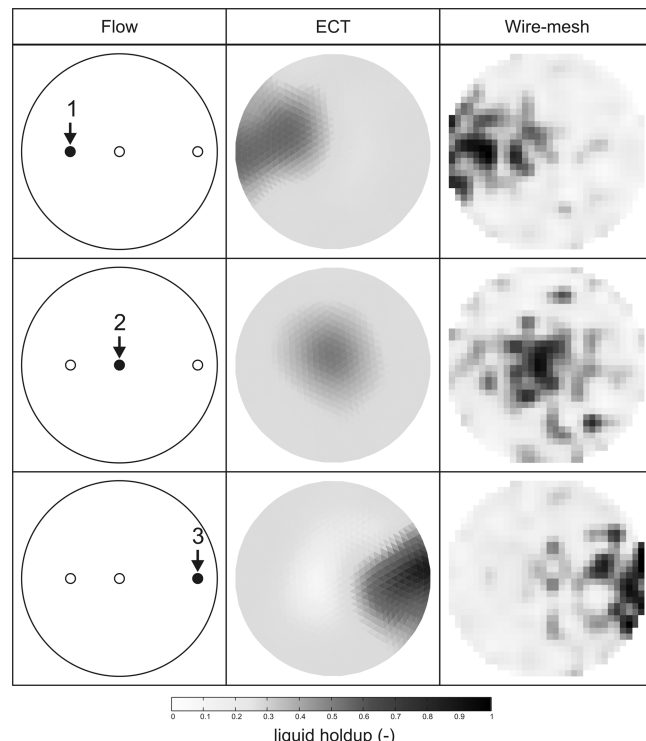


Figure 5. Images of stationary liquid distributions obtained with ECT and wire-mesh sensor.

value, the data from both modalities are normalized according to the parallel capacitor model, which assumes a linear dependence of holdup and permittivity values.⁴⁰ With this model the normalized capacitance value $C^{(n)}$ is computed via

$$C_{i,j}^{(n)} = \frac{C_{i,j}^{(\text{meas})} - C_{i,j}^{(\text{empty})}}{C_{i,j}^{(\text{flooded})} - C_{i,j}^{(\text{empty})}} \quad (6)$$

where $C^{(\text{meas})}$ is the capacitance reading for the given measurement at ECT respectively wire-mesh electrodes i, j . The normalized measurements are input to the computation of permittivity images according to eq 3 for ECT or eq 5 for the wire-mesh sensor. Following the ECT notation, we consider the computed permittivity image as a column vector \mathbf{G} with pixels G_k . Given this image we may calculate the integral liquid holdup in the cross section as an area-weighted average in the form

$$h = \frac{\sum_{k=0}^{N-1} A_k G_k}{\sum_{k=0}^{N-1} A_k} \quad (7)$$

where A_k is the area of the pixel k (note that ECT pixels are not square).

3. Results and Discussion

3.1. Steady Flow Measurements. The liquid distribution of a steady flow was investigated for different inlet positions. Thus, stationary liquid distribution measurements were simultaneously performed with the wire-mesh sensor and ECT for 20 s. One scan for inflow at each one of the three inlets and with two different volumetric liquid flow rates of 40 and $60 \text{ L} \cdot \text{h}^{-1}$ was made. Figure 5 shows images for flows with a volumetric liquid flow rate of $40 \text{ L} \cdot \text{h}^{-1}$. These images are time-averaged over

Table 2. Comparison of Holdups (%) for Different Inlet Operations and Flow Rates

	flow 1		flow 2		flow 3		
	static	40 L·h ⁻¹	60 L·h ⁻¹	40 L·h ⁻¹	60 L·h ⁻¹	40 L·h ⁻¹	60 L·h ⁻¹
ECT	19.0	26.8	32.1	26.6	33.6	26.1	30.5
WMS	19.5	26.1	30.4	28.6	32.8	26.7	28.9
Δ^a	0.5	0.7	1.7	2.0	0.8	0.6	1.6

^a Absolute difference in holdups calculated from ECT and wire-mesh sensor (WMS).

20 s. The lack of spatial resolution for the ECT images is obvious. However, the shapes of liquid distributions in the ECT images are in very good agreement with corresponding ones in

the wire-mesh sensor images. In the cases of inlet 1 and 3 operation, the ECT images show a liquid holdup in the center which is too low. This is interpreted as the result of a nonadequate model for data normalization.

Table 2 presents the comparison of the cross-section-integrated holdups calculated on the base of the liquid distribution images. The differences in the holdup values for the different modalities are smaller than 2%, which proves that both methods give quite similar results.

3.2. Dynamic Flow Measurements. An unsteady flow was induced by manually opening and closing only one of the three available liquid inlets. Liquid distribution images as well as time series of holdup measurements from both sensors were eval-

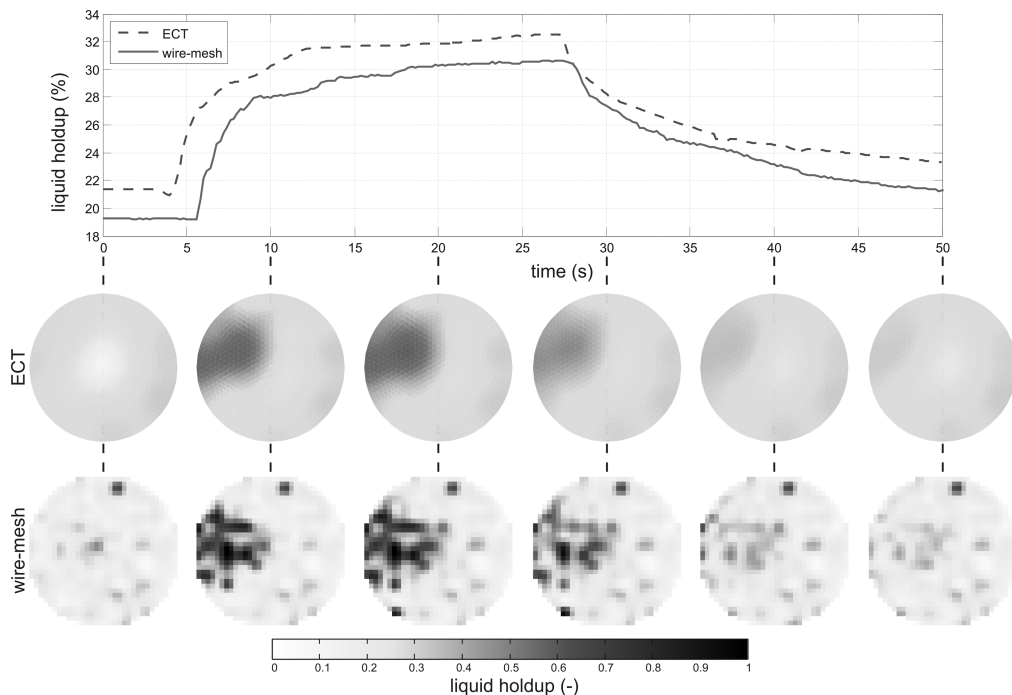


Figure 6. Liquid holdup and distribution for an oscillating flow of $60 \text{ L}\cdot\text{h}^{-1}$ from inlet 1.

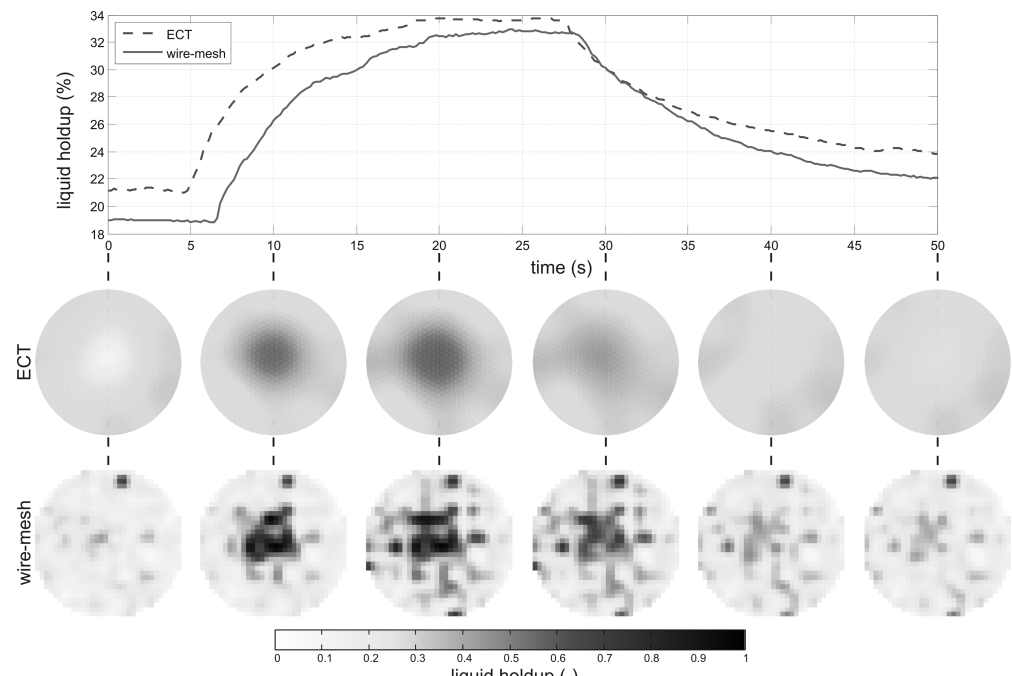


Figure 7. Liquid holdup and distribution for an oscillating flow of $60 \text{ L}\cdot\text{h}^{-1}$ from inlet 2.

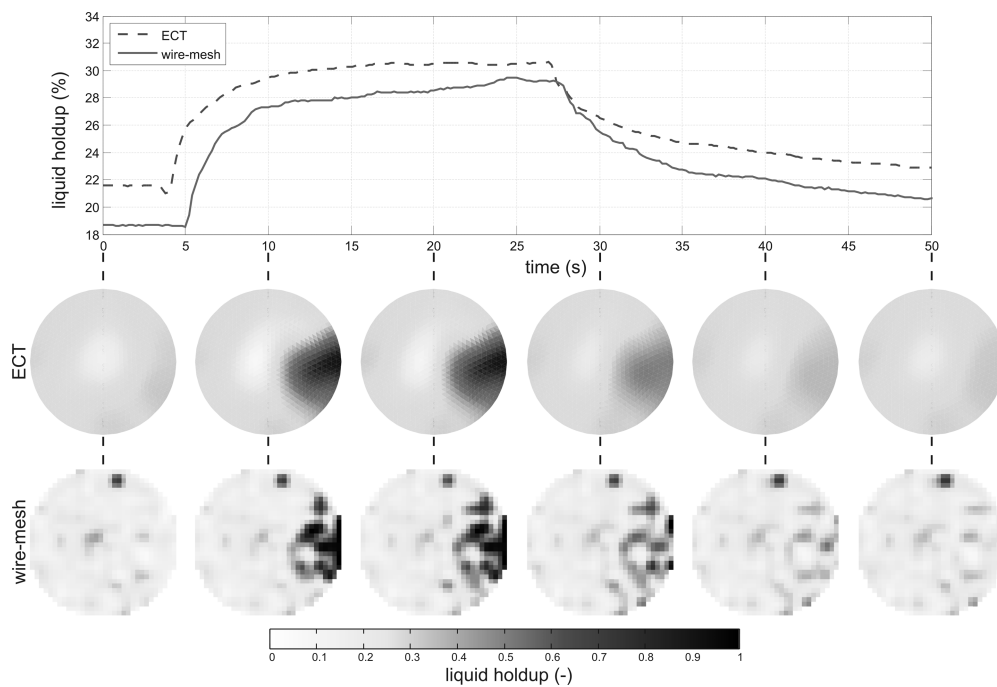


Figure 8. Liquid holdup and distribution for an oscillating flow of $60 \text{ L} \cdot \text{h}^{-1}$ from inlet 3.

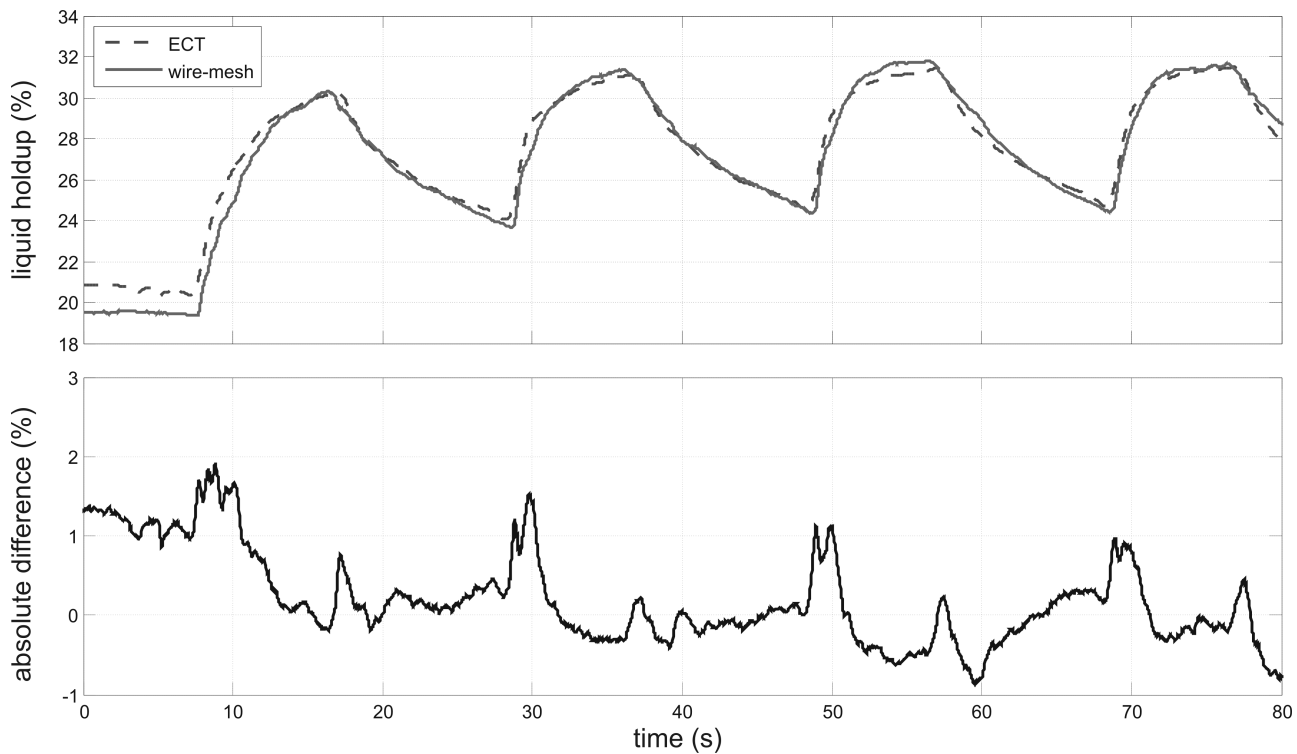


Figure 9. Liquid holdup and difference graph for intermittent flow of $40 \text{ L} \cdot \text{h}^{-1}$ from inlet 2 (holdup graph from wire-mesh sensor shifted by -1.5 s).

ated. As for the stationary measurements, all the data were recorded simultaneously with both modalities. For each one of the three inlets an on–off flow was generated. Starting the data acquisition with a zero flow, at the time of 10 s the inlet was opened for 20 s and then closed. The applied volumetric flow rate was $60 \text{ L} \cdot \text{h}^{-1}$. The liquid distribution images and holdup graphs are shown in Figures 6–8. The time courses of the liquid holdup are very similar, as are the cross-sectional liquid distributions. The plots further clearly show the expected time shift in the signals which originates from the axial sensor displacement.

For a better analysis of the differences between the holdups calculated from both modalities, an intermittent flow pattern was produced by cyclically opening and closing the second inlet with a period of 10 s. Two sequences were recorded, one with volumetric liquid flow rate of $40 \text{ L} \cdot \text{h}^{-1}$ and a second with $60 \text{ L} \cdot \text{h}^{-1}$. As both sensors are mounted at different axial positions of the column, the measured holdup curves have a temporal offset. This offset was removed in Figures 9 and 10 to make the interpretation of the data easier. Thus, the holdup graphs from the wire-mesh sensor were shifted by -1.5 s in both figures. The trends of the holdup are almost equal. The absolute

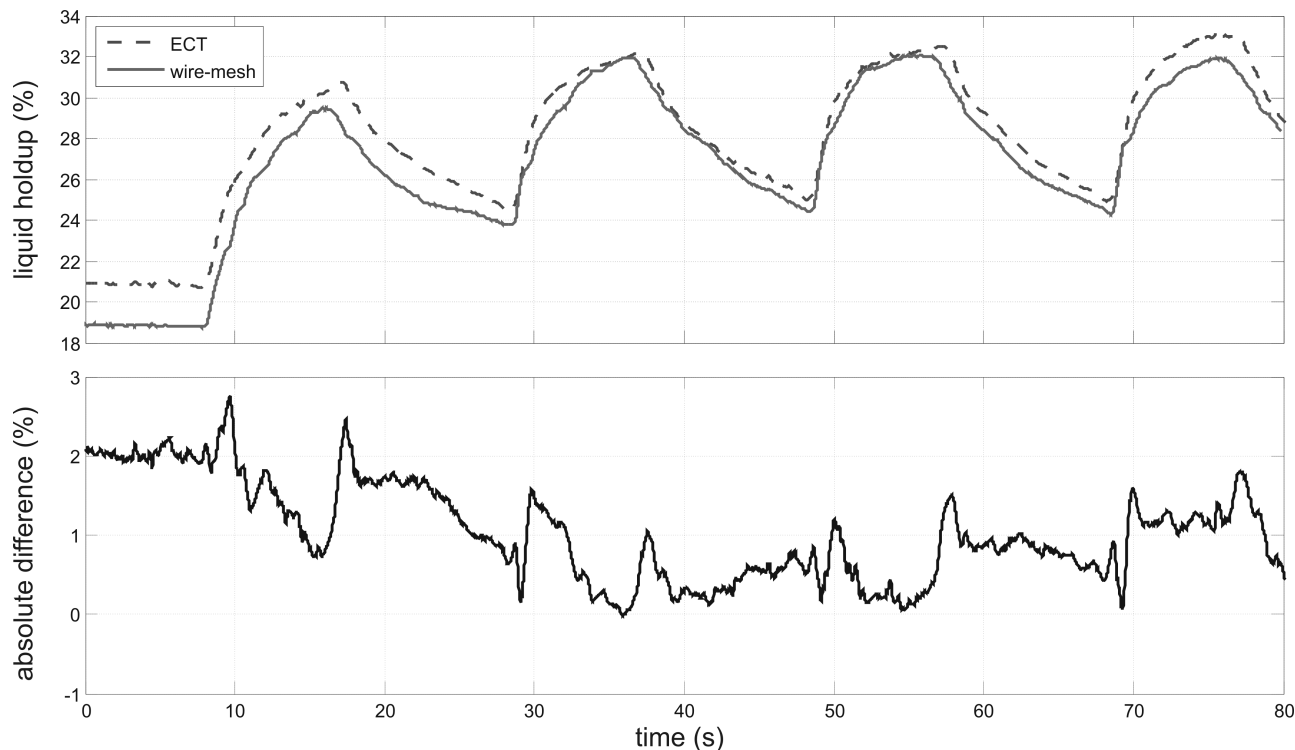


Figure 10. Liquid holdup and difference graph for intermittent flow of $60 \text{ L} \cdot \text{h}^{-1}$ from inlet 2 (holdup graph from wire-mesh sensor shifted by -1.5 s).

difference is not larger than 2.9% and is increasing whenever the flow pattern changes rapidly. This is due to the fact that ECT is axially averaging the holdup across a range of about 50 mm, whereas the wire-mesh sensor measures instantaneously within a slice of 1.5 mm. For this very reason, the differences for a volumetric flow rate of $60 \text{ L} \cdot \text{h}^{-1}$ are somewhat larger.

4. Conclusions

A capacitance wire-mesh sensor has been used for the first time to visualize the two-phase hydrodynamics in a fixed bed. The measurements were compared with electrical capacitance tomography, which can be considered an established imaging technology for multiphase flow. Both techniques have their advantages and drawbacks with respect to this application. The wire-mesh sensor scans the flow cross section with a very high spatial resolution and measures the electrical fluid properties in a direct way; i.e., no time-consuming image reconstruction is required. However, the wire-mesh sensor is also an invasive and intrusive instrument which may influence the flow and the bed packing. ECT is less intrusive; however, images are of low spatial resolution and an additional image reconstruction step is required, whose complexity rises with the required accuracy. Regarding acquisition speed and costs, the systems are comparable.

The conducted experimental study proved the usability of both sensors for measurement of liquid distributions and holdup in a fixed bed. With respect to cross-sectional liquid holdup, we demonstrated that wire-mesh sensor and ECT perform equally well. With respect to the assessment of liquid distribution, the high spatial resolution of the wire-mesh reveals much more flow detail and allows study of local flow properties deep in the bed. With ECT only coarse maldistributions of the liquid can be identified, but this is often sufficient in practical applications. It should also be noted that ECT reconstructions may be further improved by application of more sophisticated reconstruction algorithms. However, the spatial resolution limit, which is given

by the diffuse electrical field propagation in the bed, is far below that of wire-mesh sensors. As a conclusion, toward a practical application we would state that the wire-mesh sensor is to be preferred, when the focus is on ultimate spatial resolution, such as in laboratory studies, and ECT should be used whenever nonintrusive measurement is of primary importance. However, practical applications will be demanding for both types of sensors, with respect to sensor technology. Here, problems of cable feed-through, electrode and wire materials, explosion safety, etc. have to be solved.

Nomenclature

A	= pixel weight
a	= wire-mesh sensor electronics constant
b	= wire-mesh sensor electronics constant
C	= capacitance measurements vector
C	= electrical capacitance (F)
G	= permittivity image
\hat{G}	= LBP reconstructed image
H	= filter kernel for the LBP algorithm
h	= holdup distribution (%)
i, j	= electrode indices
k	= pixel index
k_g	= geometry factor
N	= number of pixels in the image
S	= sensitivity matrix
V	= output voltage of the wire-mesh sensor electronics (V)
x, y	= spatial coordinates
ϵ_r	= relative electrical permittivity
ϵ_0	= absolute electrical permittivity of vacuum ($8.85 \text{ pF} \cdot \text{m}^{-1}$)
φ	= electrical potential (V)
Γ	= area

Literature Cited

- (1) Dudukovic, M. P.; Larachi, F.; Mills, P. L. Multiphase reactors revisited. *Chem. Eng. Sci.* **1999**, *54*, 1975.

- (2) Meyers, R. A. *Handbook of petroleum refining processes*, 2nd ed.; McGraw-Hill: New York, 1996.
- (3) Saroha, A. K.; Nigam, K. D. P. Liquid Distribution in Trickle-Bed Reactors. *AICHE J.* **1998**, *44* (9), 2044.
- (4) Saroha, A. K.; Nigam, K. D. P. Trickle bed reactors. *Rev. Chem. Eng.* **1996**, *12*, 207.
- (5) Dudukovic, M. P. Opaque multiphase reactors: experimentation, modeling and troubleshooting. *Oil Gas Sci. Technol.* **2000**, *54*, 135.
- (6) Krishna, R.; Sie, S. T. Strategies for multiphase reactor selection. *Chem. Eng. Sci.* **1994**, *49*, 4029.
- (7) Marcandelli, C.; Lamine, A. S.; Bernard, J. R.; Wild, G. Liquid distribution in trickle bed reactor. *Oil Gas Sci. Technol.* **2000**, *55*, 407.
- (8) Urseanu, M. I.; Boelhouwer, J. G.; Bosman, H. J. M.; Schrojen, J. C.; Kwant, G. Estimation of trickle-to-pulse flow regime transition and pressure drop in high-pressure trickle bed reactors with organic liquids. *Chem. Eng. J.* **2005**, *111* (1), 5.
- (9) Ring, Z. R.; Missen, R. W. Trickle-bed reactors. Tracer study of liquid holdup and wetting efficiency at high temperature and pressure. *Chem. Eng.* **1991**, *69*, 1016.
- (10) Sapre, A. V.; Anderson, D. H.; Krambeck, F. J. Heater probe technique to measure flow maldistribution in large scale trickle bed reactors. *Chem. Eng. Sci.* **1990**, *45* (8), 2263.
- (11) Lazzaroni, C. L.; Keselman, H. R.; Figoli, N. S. Colorimetric evaluation of the efficiency of liquid-solid contacting in trickle flow. *Ind. Eng. Chem. Res.* **1988**, *27*, 1132.
- (12) Gladden, L. F.; Alexander, P.; Britton, M. M.; Mantle, M. D.; Sederman, A. J.; Yuen, E. H. L. In situ magnetic resonance measurement of conversion, hydrodynamics and mass transfer during single- and two-phase flow in fixed-bed reactors. *Magn. Reson. Imag.* **2003**, *21*, 213.
- (13) Gladden, L. F.; Lim, H. H. M.; Mantle, M. D.; Sederman, A. J.; Stitt, E. H. MRI visualisation of two-phase flow in structured supports and trickle-bed reactors. *Catal. Today* **2003**, *79–80*, 203.
- (14) Koptyug, I. V.; Lysova, A. A.; Sagdeev, R. Z.; Kirillov, V. A.; Kulikov, A. V.; Parmon, V. N. In situ MRI of the structure and function of multiphase catalytic reactors. *Catal. Today* **2005**, *105*, 464.
- (15) Nguyen, N. L.; Van Buren, V.; Von Garnier, A.; Hardy, E. H.; Reimert, R. Application of magnetic resonance imaging (MRI) for investigation of fluid dynamics in trickle bed reactors and of droplet separation kinetics in packed beds. *Chem. Eng. Sci.* **2005**, *60*, 6289.
- (16) Marchot, P.; Toye, D.; Pelsser, A.-M.; Crine, M.; L'Homme, G.; Olujic, Z. Liquid distribution images on structured packing by X-ray computed tomography. *AICHE J.* **2001**, *47*, 1471.
- (17) Van der Merwe, W.; Nicola, W.; De Beer, F. Trickle flow distribution and stability by X ray radiography. *Chem. Eng. Sci.* **2007**, *132*, 47.
- (18) Boyer, C.; Koudila, A.; Chena, P.; Dudukovic, M. P. Study of liquid spreading from a point source in trickle bed via gamma-ray tomography and CFD simulation. *Chem. Eng. Sci.* **2005**, *60*, 6279.
- (19) Schubert, M.; Hessel, G.; Zippe, C.; Lange, R.; Hampel, U. Liquid flow texture analysis in trickle bed reactors using high-resolution gamma ray tomography. *Chem. Eng. J.* **2008**, *140*, 332.
- (20) Dickin, F.; Wang, M. Electrical resistance tomography for process applications. *Meas. Sci. Technol.* **1996**, *7*, 247.
- (21) Reinecke, N.; Mewes, D. Recent developments and industrial/research applications of capacitance tomography. *Meas. Sci. Technol.* **1996**, *7*, 233.
- (22) Yang, W. Q.; Peng, L. Image reconstruction algorithms for electrical capacitance tomography. *Meas. Sci. Technol.* **2003**, *14*, R1.
- (23) Reinecke, N.; Mewes, D. Tomographic Imaging of Trickle-Bed Reactors. *Chem. Eng. Sci.* **1996**, *51*, 2131.
- (24) Reinecke, N.; Mewes, D. Investigation of the two-phase flow in trickle-bed reactors using capacitance tomography. *Chem. Eng. Sci.* **1997**, *52*, 2111.
- (25) Reinecke, N.; Mewes, D. Multielectrode Capacitance Sensors for the Visualization of Transient Two-Phase Flows. *Exp. Therm. Fluid Sci.* **1997**, *15*, 253.
- (26) Tibirna, C.; Edouard, D.; Fortin, A.; Larachi, F. Usability of ECT for quantitative and qualitative characterization of trickle-bed flow dynamics subject to filtration conditions. *Chem. Eng. Process.* **2006**, *45*, 538.
- (27) Hamidipour, M.; Larachi, F.; Ring, Z. Monitoring Filtration in Trickle Beds Using Electrical Capacitance Tomography. *Ind. Eng. Chem. Res.* **2009**, *48* (3), 1140.
- (28) Warsito, W.; Fan, L. S. ECT imaging of three-phase fluidized bed based on three phase capacitance model. *Chem. Eng. Sci.* **2003**, *58*, 823.
- (29) Prasser, H. M.; Böttger, A.; Zschau, J. A new electrode-mesh tomograph for gas liquid flows. *Flow Meas. Instrum.* **1998**, *9*, 111.
- (30) Hampel, U.; Otahal, J.; Boden, S.; Beyer, M.; Schleicher, E.; Jicha, M. Miniature conductivity wire-mesh sensor for gas-liquid two-phase flow measurement. *Flow Meas. Instrum.* **2009**, *20*, 15.
- (31) Llamas, J. D.; Péret, C.; Lesage, F.; Weber, M.; D'Ortona, U.; Wild, G. Wire mesh tomography applied to trickle beds: A new way to study liquid maldistribution. *Chem. Eng. Process.* **2008**, *47*, 1765.
- (32) Llamas, J. D.; Lesage, F.; Wild, G. Influence of Gas Flow Rate on Liquid Distribution in Trickle-Beds Using Perforated Plates as Liquid Distributors. *Ind. Eng. Chem. Res.* **2009**, *48* (1), 7.
- (33) Da Silva, M. J.; Schleicher, E.; Hampel, U. Capacitance wire-mesh sensor for fast measurement of phase fraction distributions. *Meas. Sci. Technol.* **2007**, *18*, 2245.
- (34) Lide, D. R. *CRC Handbook of Chemistry and Physics*, 86th ed.; CRC Press: Boca Raton, 2005.
- (35) Gianetto, A.; Specchia, V. Trickle-bed reactors: state of art and perspectives. *Chem. Eng. Sci.* **1992**, *47*, 3197.
- (36) Olszewski, T.; Kleczyński, P.; Brzeski, P.; Mirkowski, J.; Pląskowski, A.; Smolik, W.; Szabatin, R. Electrical capacitance tomograph design. *3rd International Symposium on Process Tomography in Poland, Łódź*, 2004.
- (37) Yang, W. Q.; York, T. A. New AC-based capacitance tomography system. *IEE Proc.: Sci. Meas. Technol.* **1999**, *146*, 47.
- (38) Jaworski, A. J.; Bolton, G. T. The design of an electrical capacitance tomography sensor for use with media of high dielectric permittivity. *Meas. Sci. Technol.* **2000**, *11*, 743.
- (39) Wajman, R.; Mazurkiewicz, Ł.; Banasiak, R. The sensitivity map in the image reconstruction process for Electrical Capacitance Tomography. *3rd International Symposium on Process Tomography in Poland, Łódź*, 2004.
- (40) McKeen, T. R.; Pugsley, T. S. The influence of permittivity models on phantom images obtained from electrical capacitance tomography. *Meas. Sci. Technol.* **2002**, *13*, 1822.

Received for review June 18, 2009
 Revised manuscript received November 25, 2009
 Accepted December 17, 2009

IE900988F